nature materials

PERSPECTIVE

https://doi.org/10.1038/s41563-020-0734-4

Chiral metal surfaces for enantioselective processes

Nisha Shukla[1,2] and Andrew J. Gellman[2,3] ✉

Chiral surfaces are critical components of enantioselective heterogeneous processes such as those used to prepare enantiomerically pure pharmaceuticals. While the majority of chiral surfaces in practical use are based on achiral materials whose surfaces have been modified with enantiomerically pure chiral adsorbates, there are many inorganic materials with valuable surface properties that could be rendered enantiospecific, if their surfaces were intrinsically chiral. This Perspective discusses recent developments in the fabrication of intrinsically chiral surfaces exhibiting enantiospecific adsorption, surface chemistry and electron emission. We propose possible paths to the scalable fabrication of high-surface-area, enantiomerically pure surfaces and discuss opportunities for future progress.

Chiral surfaces serve as environments for a variety of heterogeneous enantioselective processes used in industries such as pharmaceuticals and agrochemicals, and others that produce enantiomerically pure bioactive compounds. Perhaps the most common use of chiral surfaces is as stationary phases in chromatographic enantiomeric separations of chiral compounds[1–3]. In principle, chiral surfaces can be used for numerous other enantiospecific chemical and physical processes, including heterogeneous catalysis, enantiospecific sensing, crystallization, electron spin polarization and so on[4–11]. While the majority of chiral surfaces currently in use are based on the modification of otherwise achiral surfaces with chiral organic adsorbates, there are many inorganic materials, including metals and semiconductors, that can expose intrinsically chiral surfaces with enantiospecific properties that are inaccessible to organically modified surfaces[12,13]. Metals, for example, have unique catalytic properties, while semiconductors can be used for sensing applications. One of the key challenges to the development of practically useful, intrinsically chiral, inorganic surfaces is their production by methods that are scalable. In this Perspective, we summarize the current state of the art in the preparation of naturally chiral metal surfaces by means that are potentially scalable, and we provide commentary on likely avenues of progress in the near future.

While the bulk structures of many oxides, minerals and other inorganic crystalline phases are chiral, the bulk structures of metals are not. Nonetheless, the surface of a metal crystal, M(*hkl*), can be chiral, if its surface normal does not lie in any of the mirror planes of the bulk crystal lattice; or equivalently, its Miller indices obey $h \neq k \neq l \neq k$ and $h \times k \times l \neq 0$ (refs. [6,12–18]). Consider the stereographic projection shown in Fig. 1 as a construct for representation of all possible surface orientations in a face-centred cubic (fcc) lattice. All of the points on the interior of the triangle represent chiral surfaces, while those on the perimeter are achiral. The chiral surfaces have structures formed by the intersection of terraces, steps and kinks that are microfacets of the low-Miller-index (111), (110) and (100) bulk crystal planes. The handedness of such surfaces can be assigned by conventions that consider the sense of rotation (clockwise or anticlockwise) of the low-Miller-index microfacets about the kink; or equivalently, the rotational sense of the high-symmetry, low-Miller-index directions around the surface normal[12,13,19,20]. The vast majority of such intrinsically chiral surfaces that have been studied over the two decades since their discovery, have been metal single crystals suitable for scientific investigation, but not of practical utility[6,13,15]. Intrinsically chiral metal surfaces have demonstrated a wide variety of enantiospecific interactions with chiral adsorbates. Chiral molecules have enantiospecific adsorption energies[21–23] and orientations[16,24–26] on chiral metal surfaces. Exposure of chiral metal surfaces to racemic mixtures can lead to enantioselective separations based on their enantiospecific adsorption energies[27–29]. Reactions of chiral adsorbates on chiral surfaces exhibit enantiospecific rates[30–32]. Recently, it has been shown that reaction mechanisms such as surface explosions with nonlinear kinetics can lead to extremely highly enantiospecific rates[33–35].

The design and development of chiral surfaces for enantiospecific applications faces two fundamental challenges. The first is identification of materials and surfaces having optimal enantiospecific interactions with chiral compound(s) of interest[36,37]. The second challenge is the scalable preparation of those chiral surfaces in useful quantities and morphologies. While chiral surface design is an interesting and active area of research, this perspective concerns the latter, which has seen substantial developments in recent years. Enantioselective surface chemistry is, in some sense, the quintessential example of structure-sensitive surface chemistry. The two enantiomers of a chiral metal surface, M(*hkl*)^R and M(*hkl*)^S are chemically identical in their interactions with achiral adsorbates. Their only characteristic that imparts enantioselectivity is the lack of structural mirror symmetry. That being the case, one of the key challenges in chiral surface science is the identification of those chiral surface orientations that maximize their enantiospecific interactions with chiral adsorbates[37]. While computational approaches could be useful to address such issues, the relatively small (a few kilojoules per mole) differences in the enantiospecific energetics of chiral adsorbates with chiral surfaces[21,28] make such assessment challenging. This unfortunately limits the potential contribution of computational simulations to chiral surface design, and requires careful experimental characterization of enantiospecific adsorbate–surface interactions and chemistry. Some progress towards identification of chiral surface structures with optimized

[1]Institute for Complex Engineered Systems, Carnegie Mellon University, Pittsburgh, PA, USA. [2]Department of Chemical Engineering, Carnegie Mellon University, Pittsburgh, PA, USA. [3]W.E. Scott Institute for Energy Innovation, Carnegie Mellon University, Pittsburgh, PA, USA. ✉e-mail: gellman@cmu.edu

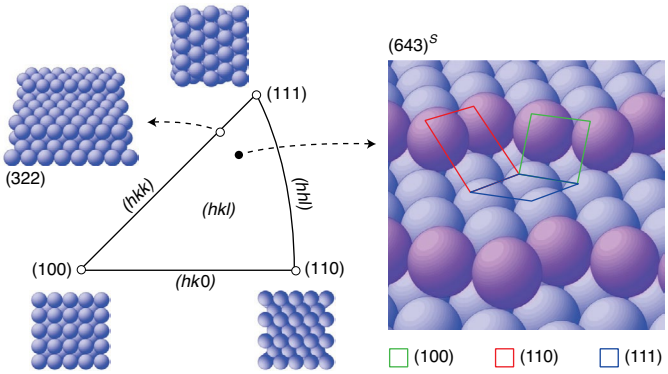

Fig. 1 | Chirality of metallic crystal surfaces. The stereographic projection (triangle) enumerating all possible surface orientations of an fcc lattice with illustrations of the three high-symmetry, achiral, low-Miller-index planes represented by the vertices of the triangle. The edges represent achiral surfaces such as (322) with low-Miller-index terraces separated by straight step edges. The points in the interior represent the low-symmetry, chiral surfaces with high Miller indices. The fcc(643)^S surface representation highlights the structural motif of three low-Miller-index microfacets (terrace, step and kink) intersecting around the kink. Their rotational sense about the surface normal defines the handedness of the chiral surface. The purple atoms highlight the kinked step edges separating (111) terraces.

enantiospecific properties is being made experimentally by using spherical single crystals that expose continuous distributions of surface orientations such that hundreds of surface orientations can be studied simultaneously[36–38].

The second challenge to the practical implementation of chiral metal surfaces and the subject of this Perspective is the development of methods for their scalable production in forms that have usable surface areas. This is a fairly nascent problem. Most of the progress made in understanding chiral surface chemistry has been based on the use of small (about 1 cm^2) single crystals that can be prepared in the laboratory or purchased from suppliers of scientific materials. While these can be used for some applications that require only low-surface-area formats, such as enantiomer sensing, chemical processes such as separations and catalysis require large functional surface areas. In this Perspective, we evaluate the progress of various strategies for the preparation of chiral metal surfaces in high-surface-area form. Some of these strategies have been demonstrated at the proof-of-concept level, while others have not (yet). In any case, all of these offer exciting opportunities for future developments.

Homochiral heteroepitaxial growth of chiral metal films

There are a number of abundant inorganic materials and minerals that have chiral bulk structures or expose chiral surface orientations that could serve as substrates for growth of chiral metal films[39]. The deposition of metal films onto chiral substrates or under conditions that impose some type of symmetry breaking (chiral solvent, reagent and so on) has been demonstrated to yield thin films with chiral surface orientations. The first attempt used pulsed laser deposition to deposit Pt and Cu thin films onto $SrTiO_3$(621) (refs. [40,41]). $SrTiO_3$ is closely lattice matched (0.5%) with Pt and therefore a good substrate for its epitaxial growth. Although the bulk structure of $SrTiO_3$ is achiral, its (621) surface is a low-symmetry, chiral surface. One of the challenges encountered during initial attempts to grow Pt epitaxially on a $SrTiO_3$ substrate was the tendency of the Pt film to dewet from the substrate surface and grow as islands during high-temperature deposition. The strategy for overcoming this was to deposit very thin films at high temperature to induce purposeful formation of small epitaxial single-crystalline nuclei. Once these nuclei had formed, further deposition at low temperature formed a non-epitaxial, poorly ordered film over the crystalline nuclei. Subsequent high-temperature annealing resulted in the formation of crystalline, epitaxial Pt films. Salvador et al. demonstrated that the deposition of Pt and Cu onto a $SrTiO_3$(621) substrate yielded 100-nm-thick Pt and Cu films, which were shown via their X-ray diffraction (XRD) pole figures to be epitaxial and oriented along the (621) direction[40,41]. Low-energy electron diffraction on the Pt(621) film revealed split diffraction spots that are indicative of its termination by a low-symmetry, high-Miller-index, chiral surface. This first demonstration of homochiral, heteroepitaxial growth demonstrated that, in principle, the deposition of metals onto chiral minerals such as quartz, even in particulate form, could be used as a route to preparation of chiral metals in high-surface-area morphologies.

Switzer et al. have demonstrated the homochiral electrodeposition of CuO onto a variety of achiral metal surfaces, including Au(001), Cu(110) and Cu(111)[42–45]. These substrate surfaces are achiral, so the chirality of the CuO films is controlled by chiral species in the electrodeposition solution. On the Au(001) surface, CuO films grow with the CuO($1\bar{1}\bar{1}$) orientation from solutions containing *S*,*S*-tartrate and with the CuO($\bar{1}11$) orientation from solutions containing *R*,*R*-tartrate. CuO($1\bar{1}\bar{1}$) and CuO($\bar{1}11$) are chiral enantiomorphs of one another[45]. Electrodeposition from solutions containing racemic tartrate yields films with domains of both CuO($1\bar{1}\bar{1}$) and CuO($\bar{1}11$). The homochiral CuO($1\bar{1}\bar{1}$) and CuO($\bar{1}11$) films grown on Au(001) were also shown to be enantiospecific in their electrochemical oxidation of *S*,*S*-tartrate and *R*,*R*-tartrate. These results were extended recently by the demonstration that chirally oriented films of metals such as Pt, Ni, Cu and Ag can be electrodeposited onto chiral Si(643) substrates (Fig. 2)[39]. The process begins with epitaxial electrodeposition of Au onto Si(643) or Si($\bar{6}\bar{4}\bar{3}$), yielding enantiomorphous chiral Au films. These can then be modified further by electrodeposition of Pt, Ni, Cu and Ag to yield chiral surfaces of each. The orientations of the chiral films have been determined by XRD pole figures (Fig. 2). The chirality of these surfaces is also revealed by their enantiospecific electro-oxidation of D- and L-glucose. Collectively, these studies demonstrate the feasibility of growth of chiral metal surfaces by both physical and chemical deposition methods onto chiral substrates.

Chiral imprinting

It has been understood for decades that there is a dynamic relationship between the atomistic structure of a metal surface and molecules adsorbed on that surface[46,47]. Adsorbates can induce a variety of structural changes to the surfaces of metallic substrates. These include, among others, macroscopic changes to nanoparticle shape, induction or removal of atomistic surface reconstructions, faceting of surface planes, faceting of step edges, and extraction of atoms from the surface to form adatoms[46–48]. When the adsorbate is chiral, the adsorbate-induced restructuring of the metal substrate can yield chiral surfaces, with the surface chirality dependant on the chirality of the adsorbate. This is the essence of chiral imprinting; transmission of molecular chirality into the structure of a metal surface[49,50]. This is differentiated from chiral surface modification in the sense that it is not just the chirality of the adsorbed modifier that influences the enantioselectivity of reactions of chiral or prochiral co-adsorbates, it is also the induced chirality of the metal substrate. Alternatively, one can imagine that once a chiral imprinting agent has induced surface reconstruction it could, in principle, be removed from the surface, leaving an intrinsically chiral, clean metal surface.

The first clear example and recognition of chiral imprinting of a metal surface comes the work of Besenbacher et al., who used

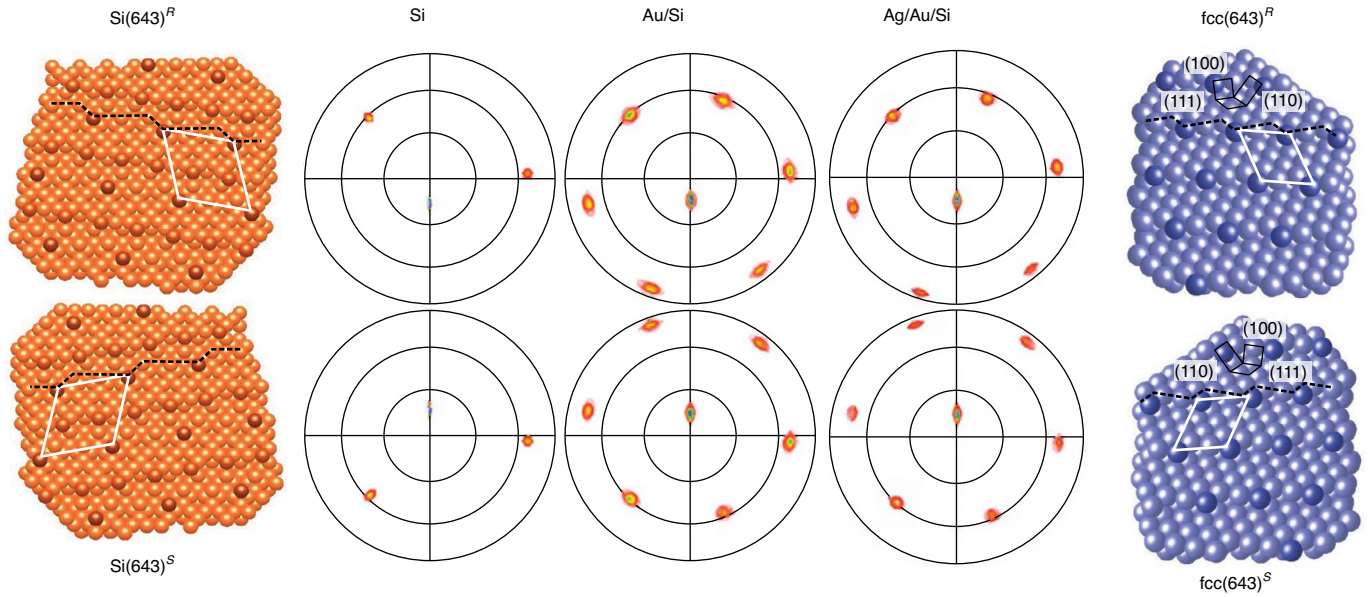

Fig. 2 | Chiral metallic surfaces fabricated by electrodeposition. Left to right: ideal structures of the chiral Si(643)$^{R\&S}$ surfaces; (111) XRD pole figures of the Si substrate, Au/Si and Ag/Au/Si films; and the ideal structures of fcc(643)$^{R\&S}$ metal surfaces. The coloured spots in the XRD pole figures indicate the regions of high scattering intensity (blue, high; yellow, intermediate; red, low). The dashed lines on the surface stuctures indicate the kinked step edges that separate the (111) teraces. The white parallelograms indicate the units cells of the surface structures. The asymmetry of the pole figures reveals the chirality of these films and the mirror relationship through the horizontal reveals the enantiomorphous relationships of the film structures on the two Si(643)$^{R\&S}$ substrate orientations[39]. The chiral fcc(643)$^{R\&S}$ metal surfaces have structures based on (111) terraces, (100) steps and (110) kinks that are projections of the three low-Miller-index planes out of the surface, which are represented at the top of each panel as black intersecting polygons. Figure adapted with permission from ref. [39], American Chemical Society.

scanning tunnelling microscopy (STM) to study the adsorption of hexa-*tert*-butyl-decacyclene (HtBDC) on Cu(110) (Fig. 3a)[51,52]. HtBDC is configurationally chiral in the sense that its chirality arises from twisting of the three peripheral naphthyl rings into the chiral geometry of a three-bladed propeller, which can be left- or right-handed. When HtBDC is adsorbed on the Cu(110) surface at 300 K, it aggregates into bimolecular rows in which all molecules in a row have the same chirality, and are readily distinguishable with STM. Use of the STM tip (at 5 K) to move the HtBDC molecules away from their preferred adsorption sites revealed that adsorption had resulted in the extraction of seven Cu atoms/HtBDC from the close-packed rows of the Cu(110) surface, leaving atomic-scale divots or trenches in the Cu(110) surface structure (Fig. 3c). These trenches in the top Cu(110) layer have shapes that are chiral with a handedness that is dictated by the chirality of the HtBDC adsorbed over them. This is true chiral imprinting in which it is demonstrably possible, albeit with an STM tip at 5 K, to remove the chiral imprinting agent (HtBDC) without loss of the chirality imprinted into the metal substrate.

Another example of chiral imprinting of a metal occurs during adsorption of the amino acid L-lysine ($HO_2CCH(NH_2)CH_2CH_2CH_2CH_2NH_2$) onto the achiral Cu(100) surface[48,53,54]. This was discovered by Zhao et al. using STM to image the surface. After adsorbing L-lysine onto the Cu(100) surface and annealing at 430 K, they observed massive reconstruction of the surface to yield Cu{3,1,17}^{R} facets separated by (100) planes covered with L-lysine (Fig. 3d). The Cu{3,1,17} planes lack mirror symmetry and are, therefore, chiral (Fig. 3e). There are eight Cu{3,1,17} planes vicinal to the Cu(100) surface; four belonging to the Cu{3,1,17}^{R} family and four to the Cu{3,1,17}^{S} family. Previous studies of several other amino acids on the Cu(100) surface had revealed reconstructions yielding all eight Cu{3,1,17} facets[48]. After adsorption of L-lysine, Zhao et al. observed only the four Cu{3,1,17}^{R} facets, indicating that L-lysine had imparted its chirality to the otherwise achiral Cu(100) surface. Later it was demonstrated that, in this case, the process of chiral imprinting is driven by the fact that the adsorption energy of L-lysine on Cu{3,1,17} is greater than its adsorption energy on Cu(100)[55]. Furthermore, the adsorption energy of L-lysine is enantiospecific, such that it is higher on Cu{3,1,17}^{R} than on Cu{3,1,17}^{S}, thus favouring the formation of Cu{3,1,17}^{R} facets during adsorption of L-lysine on Cu(100).

In most of the observed instances of chiral imprinting, the organic imprinting agent remains adsorbed to the imprinted metal surface. This limits direct contact of other adsorbing species with the intrinsically chiral metal surface and, in this regard, the imprinted surface is similar to that of a chirally modified achiral metal surface. Nonetheless, the chirality of the metal surface below the adsorbed chiral imprinting agent could amplify the enantiospecific interactions of chiral adsorbates with the imprinted surface. Ideally, one would like to remove the imprinting agent from the surface such that chiral or prochiral adsorbates can interact directly with the intrinsically chiral structure of the imprinted surface. Displacement of chiral imprinting agents represents one of the interesting challenges to chiral imprinting as a means of preparing intrinsically chiral materials. This is a difficult task. The fact that an adsorbate can reconstruct a metal surface implies that its interaction with the surface must be quite strong. Furthermore, displacement of the imprinting agent probably leaves the chiral surface in a state that is metastable, at best. Ideally, one could remove an imprinting agent by simple thermal decomposition. However, this typically results in a surface with some level of contamination resulting from decomposition of the imprinting reagent. Furthermore, heating of the imprinted metal surface typically results in lifting or loss of the chiral reconstruction to regenerate its originally achiral structure. The ideal process for removal of a chiral imprinting agent needs to leave the surface in its chirally imprinted, high-Miller-index state without

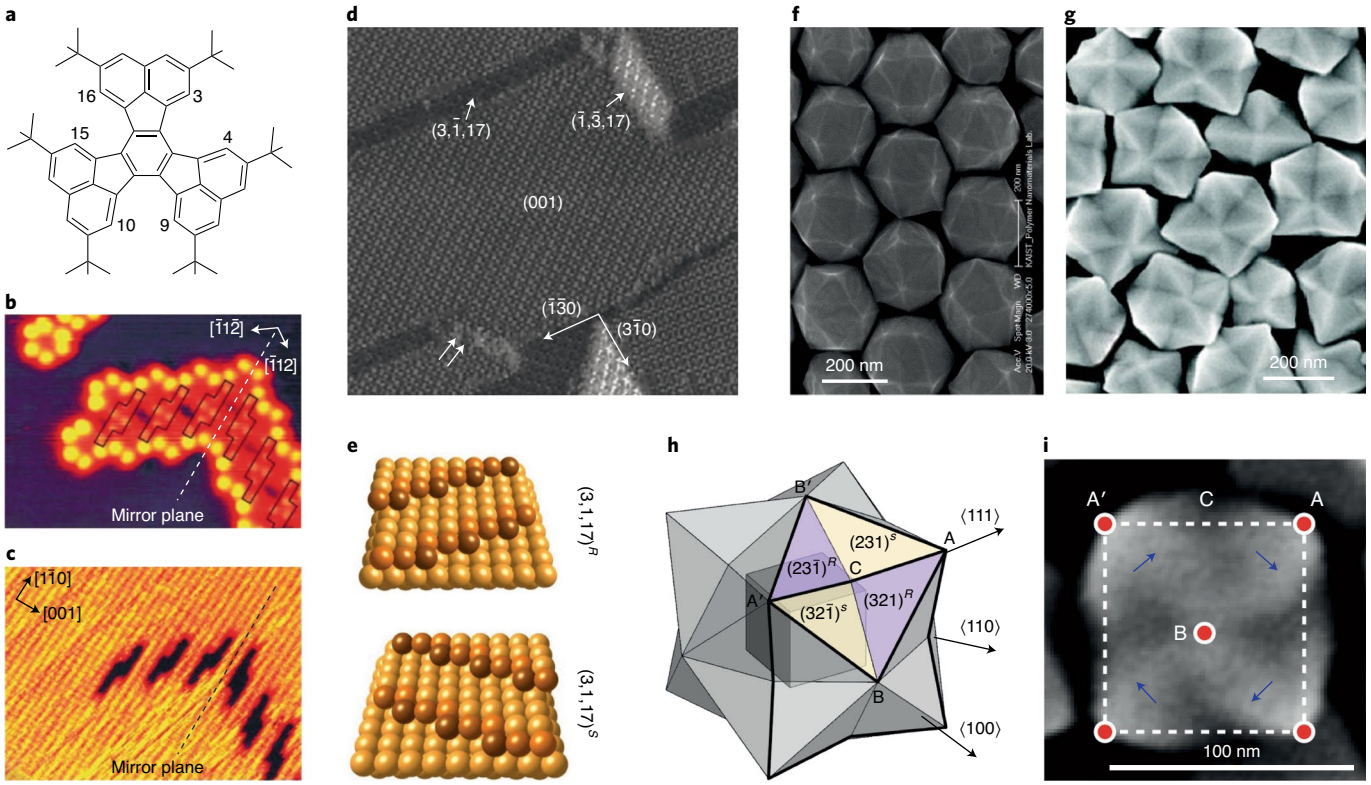

Fig. 3 | Surface restructuring methods for fabricating chiral structures. a–e, Chiral imprinting of metallic crystals. **f–i**, Metal nanoparticles with high-Miller-index facets. **a**, HtBDC. **b**, STM image (11.0 × 8.2 nm^2) of HtBDC on Cu(110). The six bright lobes on the molecule in the top left are the six tertiary butyl groups. Most molecules aggregate into bimolecular rows. **c**, STM image (11.0 × 8.2 nm^2) of the Cu(110) surface after adsorption of HtBDC at 300 K and its subsequent removal at 5 K using the STM tip. This reveals chiral trenches left by the adsorption-induced removal of Cu atoms from the rows in the Cu(110) surface. The chirality of these trenches is dictated by the chirality of the adsorbed HtBDC[51]. **d**, STM image (55.0 × 55.0 nm^2) of the Cu(100) surface following adsorption of L-lysine and annealing at 430 K. The flat terraces reveal an ordered array of L-lysine on the Cu(100) substrate. The facets belong to the Cu{3,1,17}^{R} family of surfaces. Their chirality arises from the chirality of the adsorbed L-lysine[53,54]. The two parallel arrows in the lower left show a small area of step bunching that has not resulted in the formation of a Cu{3,1,17}^{R} facet. **e**, Ideal structures of the Cu{3,1,17}$^{R\&S}$ surfaces. Atoms at the step edges are highlighted using darker colours. **f**, Micrograph of about 200-nm-diameter tetrahexahedral Au nanoparticles with achiral {520} facets[65]. **g**, About 200 nm hexoctahedral Au nanoparticles with chiral {321}$^{R\&S}$ facets[66]. **h**, Graphic of a hexoctahedral nanoparticle showing the high-symmetry, low-Miller-index crystallographic directions and the arrangement of chiral facets around the surface[68]. The labels A, B and C indicate reference features that can be found in micrograph **i**[68]. **i**, Micrograph of a Au nanoparticle grown under conditions that lead to chiral distortion and the formation of a helicoid shape. The blue arrows indicate the sense of helicity. The view is looking down the B direction relative to the illustration in **h**[68]. Panels adapted with permission from: **a–c**, ref. [51], Wiley; **d**, ref. [53], American Chemical Society; **f**, ref. [65], American Chemical Society; **g**, ref. [66], American Chemical Society; **h**,**i**, ref. [68], Springer Nature Ltd.

contamination. This probably requires a low-temperature process. For example, exposure of the imprinted surface to an adsorbate with a heat of adsorption that is greater than that of the chiral imprinting reagent could displace the imprinting reagent into the gas phase[28,29]. The ideal displacing adsorbate would be one that has a higher heat of adsorption than the imprinting agent, but at the same time has a low barrier for decomposition into fragments that desorb readily from the surface. Efforts to develop displacing agents with such characteristics are still ongoing.

Avnir et al. have scaled the concept of chiral imprinting to bulk materials through their development of organically doped metals[56,57]. These materials are prepared via reduction of metallic salts of Ag, Au or Pd in solutions containing organic compounds that can be chiral. The product is a powdered metal with the organic dopant embedded within the metal. Chiral dopants can impart enantiospecificity to the photoemission of electrons from the metal when irradiated with left- or right-handed circularly polarized light[56]. In the case of Pd doped with enantiomers of cinchona alkaloids, this chiral photoemission is preserved, even after extraction of the chiral dopant, indicating that the chirality of the dopant has been imprinted into the metal. The chirally doped Pd has also been shown to be enantioselective in its catalytic hydrogenation of prochiral isophorone, although this enantioselectivity requires the presence of the chiral alkaloid dopant[57].

Chiral nanoparticles

Chirality can be imparted to metal nanoparticles by adsorption of chiral molecular species. Many of the atomically precise Au nanoparticles prepared with monodispersed numbers of Au atoms adopt chiral structures at their surface through interaction of surface Au atoms with thiolate capping layers that pack in chiral conformations on the nanoparticle surfaces[58–60]. Not surprisingly, such chiral metal nanoparticles exhibit enantiospecific interactions with chiral compounds[61,62]. The issue of interest from the point of view of this Perspective is the preparation of such nanoparticles with intrinsically homochiral facets.

Over the past two decades there has been substantial effort worldwide focused on the chemical synthesis of metal nanoparticles with controlled size and shape. In principle, this represents a viable method for the scalable production of metals in morphologies with

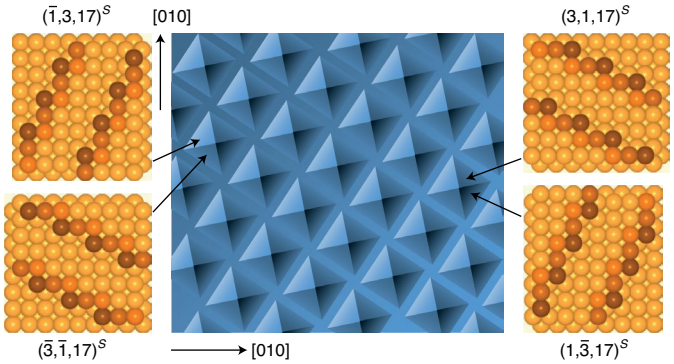

Fig. 4 | Patterning of textured metallic substrates. Graphic illustration of a M(100) RABiTS with a surface that has been patterned to have pyramidal protrusions (or pits) with four facets from the M{3,1,17}^{R} family of surfaces. The orientations of the step edges on the four facets are all superimosable by 90° rotation; that is, they are all of the same chirality. Atoms at the step edges have been highlighted by using darker colours.

naturally chiral surfaces, if nanoparticles can be grown to expose high-Miller-index planes whose chirality is limited to one enantiomer. Initial successes in metal nanoparticle synthesis yielded simple high-symmetry shapes, including spheres, cubes, tetrahedra, icosahedra and so on. Spherical particles expose surfaces of all possible crystallographic orientations, including those that are chiral, but with equal areas of both enantiomorphous orientations and, therefore, they exhibit no net chirality. The simple polyhedral shapes are all enclosed by high-symmetry, low-Miller-index planes that are achiral and tend to be favoured during growth because of their low surface energies relative to those of the less densely packed, chiral, high-Miller-index planes. In 2007, Tian et al. reported the first syntheses of metal nanoparticles with shapes enclosed by high Miller index planes[63]. These have shapes such as tetrahexahedra (24-sided, Fig. 3f) and are enclosed by surfaces with Miller indices (*hkk*), (*hhl*) or (*hk*0) that lie on the edges of the stereographic triangle. These surfaces have achiral structures based on flat, low-Miller-index terraces separated by straight monoatomic step edges (Fig. 1)[64,65]. In 2012, Hong et al. reported the synthesis of hexoctahedral (48-sided, Fig. 3g) metal nanoparticles enclosed by high-Miller-index planes with indices (*hkl*) such that $h \neq k \neq l \neq h$ and $h \times k \times l \neq 0$, that is, planes having intrinsically chiral atomic structures (Fig. 3h)[66,67]. However, these hexoctahedral nanoparticles have no net chirality because 24 of the 48 faces have *R* chirality while the remaining 24 have *S* chirality. Imparting a net chirality to these nanoparticles requires biasing the growth conditions to favour one of the two surface enantiomers. Finally, in 2018, Lee et al. reported a synthesis of Au nanoparticles that results in the distortion of the hexoctahedral shape into a helicoid (Fig. 3i) whose chirality is dictated by the addition of chiral amino acids or peptides into the synthesis medium[68]. The chiral surfaces of this structure must be biased enantiospecifically. This breakthrough has the potential to yield nanoparticles of many metals exposing homochiral facets; that is, nanoparticles capable of enantioselective surface chemistry.

In addition to the nanoparticles commonly prepared by wet chemical synthesis, there are other chiral nanostructures that have been prepared by physical means. Over the past decade, helical nanostructures with dimensions of about 100 nm and pitches of about 10 nm have been prepared from a number of materials including metals by using glancing angle deposition of thin films onto rotating substrates[69,70]. In these structures the chirality of the helix is readily controlled by the direction of the rotation of the substrate. These have strong chiroptic properties and can also exhibit enantiospecific interactions with chiral molecules. This is a bit surprising given the mismatch of their dimensions with those of molecules, but suggests that the surfaces of these nanohelices expose surface adsorption sites with some net chirality. That said, they must expose a broad distribution of surface orientations including a mixture of both *R* and *S* surfaces.

Table 1 | Comparison of chiral surface preparation methods relative to surface orientation, surface area, and surface composition

Method	Surface orientation control	Surface area	Surface species
Homochiral epitaxy	High	Low	No
Chemical imprinting	Low	Medium	Yes
Chiral nanoparticle	Low	High	Yes
RABiTS impression	High	Medium	No

Impression of chiral surface orientations into textured substrates

The previous sections have described methods for scalable preparation of intrinsically chiral surfaces, each having some associated proof of concept. No doubt, there are many innovative possibilities that have yet to be articulated or realized but are feasible, in principle. As an example, one could envision a somewhat brute-force approach starting with a large-area, rolling assisted biaxially textured substrate (RABiTS)[71,72]. These are rolled foils of fcc metals such as Cu or Ni that, during extensive annealing, become textured such that they expose a {100} plane with one of the ⟨100⟩ directions oriented parallel to the rolling direction. In essence, these are very large (about 100 × 0.1 m^2) single-crystalline foils. RABiTS have been developed as substrates for the deposition of high-temperature superconductors, but also have potential for use in applications requiring large-area, single-crystalline metals. If one could cause them to form such that they adopt a chiral, low-symmetry, single enantiomer orientation vicinal to the {100} plane, RABiTS could serve as a route to the scalable production of intrinsically chiral metal surfaces. We have already pointed out that the adsorption of L-lysine on Cu(100) surfaces leads to the formation of homochiral Cu(3,1,17)^R facets (Fig. 2). Treatment of Cu RABiTS with L- or D-lysine should, therefore, be sufficient to generate large surface areas that are chemically textured to have a net chirality. Alternatively, mechanical impression or electrochemical etching could be used (before or after annealing) to create a knurled pattern of pyramidal protrusions or pits in the Cu(100) RABiTS surface (Fig. 4). If these features were rotated at some angle with respect to the high-symmetry (100) directions of the RABiTS, the faces of the pyramids or pits would expose a homochiral set of intrinsically chiral metal planes. As such, the RABiTS surface would be homochiral.

Outlook

Methods for the production of intrinsically chiral surfaces can be assessed on the basis of metrics including attainable surface area, orientation specificity and surface composition. Methods that generate chiral nanoparticles, for example, are likely to yield higher attainable specific surface areas than methods based on thin-film deposition onto chiral substrates. Surface orientation specificity refers to the ability to target the production of any desired crystallographic orientation (*hkl*) as opposed to a distribution of different orientations. Surface composition refers to whether or not the surface is produced with an organic adsorbate film that may need to be removed before use. Table 1 summarizes the merits of the four methods for chiral surface preparation with respect to attainable surface area, orientation specificity and surface composition.

Of course, there are also issues associated with cost, manufacturability and metrics that are application specific (temperature stability, environment stability and so on) that we will not try to address.

Homochiral heteroepitaxial growth is a promising method for the preparation of intrinsically chiral films of many different metals and perhaps even alloys. It does require the use of intrinsically chiral surfaces of substrates such as Si or quartz crystals. These are readily available but probably limited to producing chiral metal films with surface areas of a few tens of centimetres square. However, given the free choice of substrate orientation, homochiral epitaxial growth has the advantage that it is capable of delivering films with any targeted surface orientation, provided that film growth is truly epitaxial. Finally, as demonstrated by the recent work of Switzer et al., homochiral epitaxial growth can yield metal films free of organic modifiers[39]. These characteristics mean that once the optimal chiral metal surface orientation is identified for a given enantioselective process, chiral films of that metal can be prepared relatively straightforwardly with the desired orientation.

Chiral imprinting of metal surfaces by chiral adsorbates that induce surface reconstruction to homochiral orientations is probably the simplest of the methods described above from the point of view of manufacturing. In principle, it is amenable to preparation of very high specific surface areas (about 100 m^2), if applied to nanoparticles, nanoporous metals or the surfaces of RABiTS. In the case of L-lysine on Cu(100) discovered by Zhao et al.[53,54], imprinting yields chiral facets with a single orientation and chirality. It is likely that, applied to substrates with other orientations or a distribution of orientations, imprinting would yield chiral surfaces with a distribution of orientations with a net chirality. What is missing is an understanding of how to control imprinting to yield specific surface orientations. The science of imprinting is nascent and requires further effort. The final challenge to the use of imprinting is the fact that the chirally imprinted surface is generated with the chiral imprinting agent adsorbed to the surface. In many instances or applications, this may not be an issue. The challenge arises when the application requires removal of the imprinting agent without deconstruction of the chiral surface orientation. We have hypothesized above regarding the characteristics of an ideal displacing agent, but further work is needed to identify such a compound, or some other process by which imprinting can yield adsorbate-free chiral surface orientations.

The evolution of shape-controlled nanoparticle synthesis has led predictably to the recent synthesis of nanoparticles with chiral shapes[68]. That work yielded a helicoidal structure of Au that exhibited strong chiro-optic activity. The fact that they are nanoparticles means that they can be prepared with high specific surface area. In principle, the surfaces of these particles must exhibit some net chirality and, if their shapes are derived from distorted hexoctahedra, the surface chirality can be derived from a single chiral surface orientation (Fig. 3h). Given that the synthesis of these helicoid nanoparticles uses chiral organic compounds to induce chirality, it is likely that their surfaces are coated with these adsorbates that might require subsequent removal. It is important to note that this situation is somewhat different from that of imprinting agents used on initially achiral surfaces. In the case of the helicoid nanoparticles, the chiral bulk shape stabilizes the chirality of the surface orientation, increasing the likelihood that one could remove the chiral adsorbate layer without loss of surface chirality. Clearly, chiral nanoparticle synthesis must advance before they become practically useful; however, given the vast global effort in nanoparticle synthesis, it seems highly probable that this will occur.

The impression of chiral surface orientations into RABiTS has not yet been demonstrated but is described above to make the case that there must be numerous creative approaches to the scalable preparation of intrinsically chiral metal surfaces. One of the limitations to the use of RABiTS is that they are not commonly prepared from all metals. Cu(100) and Ni(100) seem to be the most common orientations available and can be prepared as foils with total surface areas of abut 10 m^2. One of the attractive features of this approach is that the method should be capable of creating any chiral surface orientation that is vicinal (within about 30°) to the orientation of the RABiTS surface. As in the case of the chiral nanoparticles, the chiral surface orientation should be stabilized by the macroscopic shape of the impressed RABiTS surface. Furthermore, the method does not require that the resulting surface be coated with chiral adsorbates. In essence, the impressed RABiTS surface is a giant chiral single crystal.

Intrinsically chiral surfaces of achiral materials such as metals have chemical and physical properties that are enantiospecific and, therefore, capable of discriminating between the enantiomers of chiral molecules in surface-mediated processes such as heterogeneous catalysis, adsorption, crystallization and so on. One of the challenges to exploiting the enantiospecific properties of intrinsically chiral metal surfaces is the need to prepare them in forms that expose large surface areas with control over surface orientation and composition. As suggested in this Perspective, there is good reason to believe that this can be achieved with some innovative materials processing and manufacturing. Once achieved, the remaining challenge to the implementation of intrinsically chiral surfaces in real enantiospecific processes and devices will be that of identifying which crystallographic surface orientation yields the highest enantiospecificity for the property of interest from a specific metal.

Received: 6 May 2019; Accepted: 15 June 2020;
Published online: 3 August 2020

References

1. Lang, J. C. & Armstrong, D. W. Chiral surfaces: the many faces of chiral recognition. *Curr. Opin. Colloid Interface Sci.* **32**, 94–107 (2017).
2. Ahuja, S. *Chiral Separations by Chromatography* (Oxford Univ. Press, 2000).
3. Maier, N. M., Franco, P. & Lindner, W. Separation of enantiomers: needs, challenges, perspectives. *J. Chromatogr. A* **906**, 3–33 (2001).
4. Baiker, A. Chiral catalysis on solids. *Curr. Opin. Solid State Mater. Sci.* **3**, 86–93 (1998).
5. Dressler, D. H. & Mastai, Y. Enantioselective crystallization of histidine on chiral self-assembled films of cysteine. *J. Colloid Interface Sci.* **310**, 653–660 (2007).
6. Gellman, A. J., Tysoe, W. T. & Zaera, F. Surface chemistry for enantioselective catalysis. *Catal. Lett.* **145**, 220–232 (2015).
7. Kawasaki, T. & Soai, K. Asymmetric autocatalysis triggered by chiral crystals formed from achiral compounds and chiral isotopomers. *Isr. J. Chem.* **52**, 582–590 (2012).
8. Kettner, M. et al. Chirality-dependent electron spin filtering by molecular monolayers of helicenes. *J. Phys. Chem. Lett.* **9**, 2025–2030 (2018).
9. Mastai, Y. Enantioselective crystallization on nanochiral surfaces. *Chem. Soc. Rev.* **38**, 772–780 (2009).
10. Rosenberg, R. A., Mishra, D. & Naaman, R. Chiral selective chemistry induced by natural selection of spin-polarized electrons. *Angew. Chem. Int. Ed.* **54**, 7295–7298 (2015).
11. Meemken, F. & Baiker, A. Recent progress in heterogeneous asymmetric hydrogenation of C=O and C=C bonds on supported noble metal catalysts. *Chem. Rev.* **117**, 11522–11569 (2017).
12. Jenkins, S. J. & Pratt, S. J. Beyond the surface atlas: a roadmap and gazetteer for surface symmetry and structure. *Surf. Sci. Rep.* **62**, 373–429 (2007).
13. Jenkins, S. R. *Chirality at Solid Surfaces* 1st edn (John Wiley & Sons, 2018).
14. Baber, A. E., Gellman, A. J., Sholl, D. S. & Sykes, E. C. H. The real structure of naturally chiral Cu{643}. *J. Phys. Chem. C* **112**, 11086–11089 (2008).
15. Gellman, A. J. Chiral surfaces: accomplishments and challenges. *ACS Nano* **4**, 5–10 (2010).
16. Gellman, A. J., Horvath, J. D. & Buelow, M. T. Chiral single crystal surface chemistry. *J. Mol. Catal. A* **167**, 3–11 (2001).
17. Hazen, R. M. & Sholl, D. S. Chiral selection on inorganic crystalline surfaces. *Nat. Mater.* **2**, 367–374 (2003).
18. McFadden, C. F., Cremer, P. S. & Gellman, A. J. Adsorption of chiral alcohols on "chiral" metal surfaces. *Langmuir* **12**, 2483–2487 (1996).
19. Ahmadi, A., Attard, G., Feliu, J. & Rodes, A. Surface reactivity at "chiral" platinum surfaces. *Langmuir* **15**, 2420–2424 (1999).
20. Attard, G. A. et al. Temperature effects in the enantiomeric electro-oxidation of d- and l-glucose on Pt{643}(S). *J. Phys. Chem. B* **103**, 1381–1385 (1999).

21. Gellman, A. J., Huang, Y., Koritnik, A. J. & Horvath, J. D. Structure-sensitive enantiospecific adsorption on naturally chiral Cu(*hkl*)$^{R\&S}$ surfaces. *J. Phys. Condens. Matter* **29**, 034001–034001 (2017).
22. Horvath, J. D. & Gellman, A. J. Enantiospecific desorption of *R*- and *S*-propylene oxide from a chiral Cu(643) surface. *J. Am. Chem. Soc.* **123**, 7953–7954 (2001).
23. Horvath, J. D. & Gellman, A. J. Enantiospecific desorption of chiral compounds from chiral Cu(643) and achiral Cu(111) surfaces. *J. Am. Chem. Soc.* **124**, 2384–2392 (2002).
24. Greber, T., Sljivancanin, Z., Schillinger, R., Wider, J. & Hammer, B. Chiral recognition of organic molecules by atomic kinks on surfaces. *Phys. Rev. Lett.* **96**, 056103 (2006).
25. Horvath, J. D., Baker, L. & Gellman, A. J. Enantiospecific orientation of *R*-3-methylcyclohexanone on the chiral Cu(643)$^{R\&S}$ surfaces. *J. Phys. Chem. C* **112**, 7637–7643 (2008).
26. Schillinger, R., Sljivancanin, Z., Hammer, B. & Greber, T. Probing enantioselectivity with X-ray photoelectron spectroscopy and density functional theory. *Phys. Rev. Lett.* **98**, 136102 (2007).
27. Horvath, J. D., Koritnik, A., Kamakoti, P., Sholl, D. S. & Gellman, A. J. Enantioselective separation on a naturally chiral surface. *J. Am. Chem. Soc.* **126**, 14988–14994 (2004).
28. Yun, Y. J. & Gellman, A. J. Enantioselective separation on naturally chiral metal surfaces: d,l-aspartic acid on Cu(3,1,17)$^{R\&S}$. *surfaces. Angew. Chem. Int. Ed.* **52**, 3394–3397 (2013).
29. Yun, Y. J. & Gellman, A. J. Enantiospecific adsorption of amino acids on naturally chiral Cu{3,1,17}$^{R\&S}$ surfaces. *Langmuir* **31**, 6055–6063 (2015).
30. Fleming, C., King, M. & Kadodwala, M. Highly efficient electron beam induced enantioselective surface chemistry. *J. Phys. Chem. C* **112**, 18299–18302 (2008).
31. Rampulla, D. M., Francis, A. J., Knight, K. S. & Gellman, A. J. Enantioselective surface chemistry of *R*-2-bromobutane on Cu(643)$^{R\&S}$ and Cu(531)$^{R\&S}$. *J. Phys. Chem. B* **110**, 10411–10420 (2006).
32. Rampulla, D. M. & Gellman, A. J. Enantioselective decomposition of chiral alkyl bromides on Cu(643)$^{R\&S}$: effects of moving the chiral center. *Surf. Sci.* **600**, 2823–2829 (2006).
33. Gellman, A. J. et al. Superenantioselective chiral surface explosions. *J. Am. Chem. Soc.* **135**, 19208–19214 (2013).
34. Mhatre, B. S., Dutta, S., Reinicker, A., Karagoz, B. & Gellman, A. J. Explosive enantiospecific decomposition of aspartic acid on Cu surfaces. *Chem. Commun.* **52**, 14125–14128 (2016).
35. Mhatre, B. S. et al. A window on surface explosions: tartaric acid on Cu(110). *J. Phys. Chem. C* **117**, 7577–7588 (2013).
36. de Alwis, A. et al. Surface structure spread single crystals (S^4Cs): preparation and characterization. *Surf. Sci.* **608**, 80–87 (2013).
37. Karagoz, B., Payne, M., Reinicker, A., Kondratyuk, P. & Gellman, A. J. A most enantioselective chiral surface: tartaric acid on all surfaces vicinal to Cu(110). *Langmuir* **35**, 16438–16443 (2019).
38. Reinicker, A. D. et al. Influence of step faceting on the enantiospecific decomposition of aspartic acid on chiral Cu surfaces vicinal to Cu{111}. *Chem. Commun.* **52**, 11263–11266 (2016).
39. Kelso, M. V., Tubbesing, J. Z., Chen, Q. Z. & Switzer, J. A. Epitaxial electrodeposition of chiral metal surfaces on silicon(643). *J. Am. Chem. Soc.* **140**, 15812–15819 (2018).
40. Francis, A. J., Koritnik, A. J., Gellman, A. J. & Salvador, P. A. Chiral surfaces and metal/ceramic heteroepitaxy in the Pt/$SrTiO_3$(621) system. *Surf. Sci.* **601**, 1930–1936 (2007).
41. Francis, A. J. & Salvador, P. A. Chirally oriented heteroepitaxial thin films grown by pulsed laser deposition: Pt(621) on $SrTiO_3$(621). *J. Appl. Phys.* **96**, 2482–2493 (2004).
42. Bohannan, E. W., Kothari, H. M., Nicic, I. M. & Switzer, J. A. Enantiospecific electrodeposition of chiral CuO films on single-crystal Cu(111). *J. Am. Chem. Soc.* **126**, 488–489 (2004).
43. Gudavarthy, R. V. et al. Epitaxial electrodeposition of chiral CuO films from copper(ii) complexes of malic acid on Cu(111) and Cu(110) single crystals. *J. Mater. Chem.* **21**, 6209–6216 (2011).
44. Kothari, H. M. et al. Enantiospecific electrodeposition of chiral CuO films from copper(ii) complexes of tartaric and amino acids on single-crystal Au(001). *Chem. Mater.* **16**, 4232–4244 (2004).
45. Switzer, J. A., Kothari, H. M., Poizot, P., Nakanishi, S. & Bohannan, E. W. Enantiospecific electrodeposition of a chiral catalyst. *Nature* **425**, 490–493 (2003).
46. Woodruff, D. P. Adsorbate-induced reconstruction of surfaces — an atomistic alternative to microscopic faceting. *J. Phys. Condens. Matter* **6**, 6067–6094 (1994).
47. Woodruff, D. P. Solved and unsolved problems in surface structure determination. *Surf. Sci.* **500**, 147–171 (2002).
48. Chen, Q. & Richardson, N. V. Surface facetting induced by adsorbates. *Prog. Surf. Sci.* **73**, 59–77 (2003).
49. Gellman, A. J. & Ernst, K. H. Chiral autocatalysis and mirror symmetry breaking. *Catal. Lett.* **148**, 1610–1621 (2018).
50. Lawton, T. J. et al. Long range chiral imprinting of Cu(110) by tartaric acid. *J. Phys. Chem. C* **117**, 22290–22297 (2013).
51. Schunack, M., Laegsgaard, E., Stensgaard, I., Johannsen, I. & Besenbacher, F. A chiral metal surface. *Angew. Chem. Int. Ed.* **40**, 2623–2626 (2001).
52. Schunack, M. et al. Anchoring of organic molecules to a metal surface: HtBDC on Cu(110). *Phys. Rev. Lett.* **86**, 456–459 (2001).
53. Zhao, X. Y. Fabricating homochiral facets on Cu(001) with l-lysine. *J. Am. Chem. Soc.* **122**, 12584–12585 (2000).
54. Zhao, X. Y., Zhao, R. G. & Yang, W. S. Scanning tunneling microscopy investigation of l-lysine adsorbed on Cu(001). *Langmuir* **16**, 9812–9818 (2000).
55. Cheong, W. Y. & Gellman, A. J. Energetics of chiral imprinting of Cu(100) by lysine. *J. Phys. Chem. C* **115**, 1031–1035 (2011).
56. Behar-Levy, H., Neumann, O., Naaman, R. & Avnir, D. Chirality induction in bulk gold and silver. *Adv. Mater.* **19**, 1207–1211 (2007).
57. Pachon, L. D. et al. Chiral imprinting of palladium with cinchona alkaloids. *Nat. Chem.* **1**, 160–164 (2009).
58. Gautier, C. & Burgi, T. Chiral gold nanoparticles. *ChemPhysChem* **10**, 483–492 (2009).
59. Jadzinsky, P. D., Calero, G., Ackerson, C. J., Bushnell, D. A. & Kornberg, R. D. Structure of a thiol monolayer-protected gold nanoparticle at 1.1 angstrom resolution. *Science* **318**, 430–433 (2007).
60. Zeng, C. J. & Jin, R. C. Chiral gold nanoclusters: atomic level origins of chirality. *Chem. Asian J.* **12**, 1839–1850 (2017).
61. Shukla, N., Bartel, M. A. & Gellman, A. J. Enantioselective separation on chiral Au nanoparticles. *J. Am. Chem. Soc.* **132**, 8575–8580 (2010).
62. Shukla, N. et al. Polarimetric detection of enantioselective adsorption by chiral Au nanoparticles — effects of temperature, wavelength and size. *Nanomater. Nanotechnol.* **5**, 1 (2015).
63. Tian, N., Zhou, Z. Y., Sun, S. G., Ding, Y. & Wang, Z. L. Synthesis of tetrahexahedral platinum nanocrystals with high-index facets and high electro-oxidation activity. *Science* **316**, 732–735 (2007).
64. Lee, H. E. et al. Concave rhombic dodecahedral Au nanocatalyst with multiple high-index facets for CO_2 reduction. *ACS Nano* **9**, 8384–8393 (2015).
65. Ming, T. et al. Growth of tetrahexahedral gold nanocrystals with high-index facets. *J. Am. Chem. Soc.* **131**, 16350–16351 (2009).
66. Hong, J. W., Lee, S. U., Lee, Y. W. & Han, S. W. Hexoctahedral Au nanocrystals with high-index facets and their optical and surface-enhanced Raman scattering properties. *J. Am. Chem. Soc.* **134**, 4565–4568 (2012).
67. Zhang, L. et al. Synthesis of convex hexoctahedral palladium@gold core-shell nanocrystals with {431} high-index facets with remarkable electrochemiluminescence activities. *ACS Nano* **8**, 5953–5958 (2014).
68. Lee, H. E. et al. Amino-acid- and peptide-directed synthesis of chiral plasmonic gold nanoparticles. *Nature* **556**, 360–365 (2018).
69. Deng, J. H., Fu, J. X., Ng, J. & Huang, Z. F. Tailorable chiroptical activity of metallic nanospiral arrays. *Nanoscale* **8**, 4504–4510 (2016).
70. Gibbs, J. G. et al. Nanohelices by shadow growth. *Nanoscale* **6**, 9457–9466 (2014).
71. Goyal, A. in *Second Generation HTS Conductors* (ed. Goyal, A.) Ch. 2, 347 (Springer, 2005).
72. Goyal, A., Paranthaman, M. P. & Schoop, U. The RABiTS approach: using rolling-assisted biaxially textured substrates for high-performance YBCO superconductors. *MRS Bull.* **29**, 552–561 (2004).

Acknowledgements

The authors' work in the field of chiral surface chemistry and catalysis has been funded by the US Department of Energy under grant number DE-SC0008703 and by the US National Science Foundation under grant number NSF CHE1764252.

Competing interests

The authors declare no competing interests.

Additional information

Correspondence should be addressed to A.J.G.